

Accepted version on Author's Personal Website: C. R. Koch

Article Name with DOI link to Final Published Version complete citation:

Khashayar Ebrahimi, David Gordon, Pervez Canteenwalla, and Charles R Koch. Evaluation of ASTM d6424 standard for knock analysis using unleaded fuel candidates on a six cylinder aircraft engine. page 146808742110087. doi: [10.1177/14680874211008703](https://doi.org/10.1177/14680874211008703)

See also:

https://sites.ualberta.ca/~ckoch/open_access/Ebrahimi2021.pdf

Post-print

As per publisher copyright is ©2021



This work is licensed under a
[Creative Commons Attribution-NonCommercial-NoDerivatives 4.0 International License](https://creativecommons.org/licenses/by-nc-nd/4.0/).



Article accepted version starts on the next page →

[Or link: to Author's Website](#)

Evaluation of ASTM D6424 Standard for Knock Analysis using Unleaded Fuel Candidates on a Six Cylinder Aircraft Engine

Khashayar Ebrahimi^a, David Gordon ^{a,*}, Pervez Canteenwalla^b, Charles R. Koch^a

^a*Dept. of Mechanical Engineering, University of Alberta, Edmonton, Canada*

^b*Gas Turbine Laboratory, National Research Council Canada, Ottawa, Canada*

Abstract

The ASTM D6424 standard is used for general aviation piston engine knock detection and is tested for unleaded fuel candidates. Issues are discussed regarding the identification of knocking cycles, filtering frequency bands, and the effects of down-sampling for this knock detection technique. The knock tests were performed on the Continental TSIO-520-VB engine at 12,000 ft for take-off and cruise conditions using three different fuels, the standard leaded LL100 avgas and two unleaded fuel candidates. The ASTM D6424 knock detection method has its own particular disadvantages, which are detailed and compared to other knock detection methods including the third derivative of pressure signal and discrete wavelet transform. Updates to the standard include a minimum sampling rate of 0.2 CAD. Additionally, the current standard does not contain recommendations for filtering the cylinder pressure which results in over detection of knocking cycles with the two new aviation fuel candidates tested. Recommendations are provided regarding the pressure signal processing prior to ASTM D6424 knock-characterization.

1. Introduction

In Spark Ignition (SI) engines, knock is associated with the auto-ignition of a portion of the air-fuel mixture ahead of the propagating flame front [1, 2]. This rapid heat release results in high local pressure and produces a shock wave. This shock wave causes a combustion chamber resonance that is amplified by the engine structure to produce the familiar knocking sound. Knock is an inherent problem of SI engines, and has been studied intensively in the literature [3, 4, 5, 6]. The engine's compression ratio, and the spark advance angle during operation are both limited by knock. Aircraft piston engines are widely used for aviation in North America and still use leaded fuel to limit knock intensity. The 100 octane Low-Lead (100LL)

aviation gasoline (avgas) is the fuel commonly used in aviation industry which contains lead in the form of Tetra-Ethyl Lead (TEL). The TEL additive is mainly used to modulate the aviation gasoline octane levels to avoid knock and engine failure. The addition of TEL in aviation gasoline also requires the addition of Ethylene DiBromide (EDB) as a scavenger to remove lead oxide from the combustion chamber. These additives are harmful to the environment, and began to be phased out of the automotive industry beginning in the 1970s and completely phased out in 1993 in Canada and 1996 in the United States. In Canada, piston aircraft engines are the second largest source of lead emissions, accounting for 17% of total emissions [7]. In the US, the aircraft piston engines produce 45% of all airborne lead emissions [8]. Studies indicate that near some air-

*Corresponding author: dgordon@ualberta.ca

ports, the lead concentration exceeds EPA limits [9]. Despite extensive efforts to find an unleaded replacement fuel for aircraft piston engines in the 1990s, no fuel that meets all the requirements was found. Therefore the aviation industry has been exempt from the leaded fuel ban [10]. To address these issues, the US Federal Aviation Administration (FAA) started an initiative in 2012 to find an alternative fuel to 100LL [11]. This collaboration between industry and government is known as the Piston Aviation Fuels Initiative (PAFI) [12]. The mission of the PAFI program is to evaluate unleaded fuel replacement candidates and identify those fuels able to meet the existing general aviation aircraft fleet requirements considering the production and distribution cost, availability, and environmental and health impacts of fuels [13].

In Canada, Environment and Climate Change Canada (ECCC), Transport Canada, and Canadian Owners and Pilots Association (COPA) initiated a project with the National Research Council Canada (NRC) and the University of Alberta to coordinate with the US efforts to conduct testing on the unleaded aviation fuel candidates. Currently, research has been performed to determine various alternative unleaded fuels available and their production and availability [14]. Engine testing has been done with a few varieties of these fuels [15]. Then using response surface methodology, these different fuels have been statistically examined for their performance and emissions compared to 100LL [13, 16]. This shows the importance of research, testing and, analysis of unleaded fuel replacement for general aviation.

Switching to unleaded fuels for aircraft piston engines will have the vital benefit of significantly reducing the amount of airborne lead, which will improve air quality and public health. Fuel anti-knock quality is one of the most important parameters that govern the occurrence of knock in SI engines. Since the lead additive to 100LL avgas raises the octane number, which is used to avoid harmful engine

knock, maintaining similar knock characteristics is essential for the unleaded fuel candidates. Engine knock tends to occur at high engine loads and is also a complex function of fuel chemistry. Engine knock has consequences, including induced engine vibration, increased rate of heat transfer to the cylinder walls, and physical engine damage due to an increase in thermal and mechanical stresses. Also, the engine indicated efficiency is limited by knock [1, 17, 18]. Aircraft engines present a unique challenge since they operate at high loads during takeoff and it is essential to maintain power during this critical stage of flight. Even during the cruise, comparable to highway driving of an automobile, an aircraft engine can operate at a relatively high load of 80%. Additionally, many aircraft engines operate at fixed spark timings and rely on the pilot to set the air-fuel ratio.

FAR 33, sub-part D, section 33.47 mandates aircraft piston engines to operate safely without knocking throughout the range of intended operating conditions [19]. The Advisory Circular (AC) 33.47 [20] has been used traditionally for knock detection; however, it does not mention the technique that needs to be used to meet the requirement. Knock is not only dependent on fuel properties, and other parameters like charge temperature, equivalence ratio, engine compression ratio, turbocharger boost pressure, spark timing, and combustion chamber design affects the knock intensity level [3]. However, using fuels with low anti-knock quality is the major reason for engine knock [21]. Technically, knock is determined by the temperature and pressure history of the end-gas and the anti-knock quality of the fuel, which is measured by the Motor Octane Number (MON) [22], Research Octane Number (RON) [23], and Super-Charge Performance Number (SCPN) [24]. These three indexes are measured on a highly calibrated Cooperative Fuel Research (CFR) engine [25, 26].

RON and MON are not enough to describe

the knock resistance of aviation fuels. For aviation gasoline, ASTM D 909 [24] standard specifies SCPN as a new index. SCPN is a critical fuel performance index for aviation gasoline, and it is an indication of rich mixture anti-knock quality. Aviation engine manufacturers use SCPN as a specification measurement related to the matching of fuels and engines [27]. For aviation turbo-charged piston engines, SCPN is essential, as these engines run at higher pressures for a given in-cylinder temperature compared to automotive engines. This fuel rating is determined by comparing the knock-limited power of the test fuel to the reference fuels under standard operating conditions defined in ASTM D 909[24]. The reference fuels used for this rating are PRF with 85 octane number and a mixture of iso-octane and 6.0 mL TEL per US gallon. The knock-limited power for the test fuel is compared to the blend of the reference fuels, and the SCPN for the sample is defined by interpolation of the Indicated Mean Effective Pressure (IMEP) at the air-fuel ratio that produces maximum knock-free IMEP.

Inaccurate identification of engine knock deteriorates the engine performance and reduces the engine life-time [28]. Various methods have been developed for knock detection in SI automotive engines. These methods are mainly based on in-cylinder pressure measurement, engine block vibration, and heat release analysis. In-cylinder pressure measurement is one effective way of knock intensity measurement; however, piezoelectric pressure transducers are not used for knock measurements in commercial engines due to their high cost and low durability. Indirect knock measurements using block accelerometers are typically used for knock detection in SI engines. In this way, several cylinders can be controlled using one low-cost sensor. Another method is to use the spark plug as an ionization probe. The probe detects knock through the sharp increase in ionization due to abnormal combustion. There exist other ap-

proaches based on heat loss due to knocking combustion. Such methods may not be applicable for light knock detection, and are challenging to implement for efficient engine knock detection and control [29, 30, 31]. Considering a wide variety of knock detection methods, ASTM D6424 [32] is the only standard test procedure that covers ground based octane rating procedures for SI aircraft piston engines.

One effective knock detection method uses the knock related pressure peak compared to the pressure, which corresponds to normal combustion. The increased rate of pressure rise due to knocking combustion is another method for knock detection; however, the method is not accurate as the rate of pressure rise is affected by several knock independent factors [33]. The peak in-cylinder pressure can be used as another approach for knock detection. The drawback of this method is that it relies on pressure signal post-processing and is not accurate for light knock detection [34]. The minimum value of the pressure third derivative due to the abrupt curvature change corresponds to a sharp knock pressure peak is another method for knock detection [35, 36]. Abnormal heat release due to the end-gas auto-ignition affects the rate of heat release signal. By using the gradient of heat release rate at descent as the knock index [37], end-gas auto-ignition can be detected at various intensities. Hence knock detection methods based on the rate of heat-release analysis are of interest; however, the method suffers from the high computational time that makes it difficult to be implemented for fast and real-time knock detection [38].

The knock detection methods based on frequency domain analysis are interesting as these methods can be easily developed and implemented for real-time knock detection and control [39, 40]. These methods work based on high-frequency pressure fluctuations that occur during knock as there is a strong correlation between the frequency amplitude and the amount of end-gas auto-ignition. Such knock

detection methods usually work based on the maximum amplitude of the pressure oscillation frequency. Examples are the band-pass filtering of the pressure signal over the knock frequency range [41]; Root Mean Square (RMS) of pressure oscillations [42], discrete Wavelet transform (DWT) of the knock signal [43, 44], and the integral of the absolute value of pressure oscillations [45]. A simple knock detection strategy can be developed by extracting the knock related pressure peak considering the maximum amplitude or the maximum peak-to-peak value of band-pass filtered pressure signal [46]. The DWT is another method for knock detection, and it provides the knock signal history at discrete scales within the crank angle window. Moreover, the DWT is computationally efficient, which makes it suitable for real-time knock detection. The DWT is constructed using the Multi-Resolution Technique (MLT) proposed in [47]. In this method, the signal is decomposed into a set of basis vectors of increasing scale resolution and decreasing time resolution. The MLT provides a signal analysis at different scales in which the frequency resolution is better for the low frequency at the expense of reduced time resolution and is coarser at higher frequencies but at a finer time resolution. This method applies to measured pressure signals in which low frequencies tend to develop and exist over a longer duration, whereas the high knock frequencies tend to exist for short bursts. Knock detection using DWT is of interest as it considers knock cyclic variability and identifies knocking cycles from normal cycles [48, 43].

Knock detection methods based on engine block vibration analysis are playing crucial roles in today’s engine spark timing control systems. These methods work based on the identification of the frequency range of knock induced vibrations followed by band-pass filtering of the vibration signal [49]. The frequency response methods explained above are implemented for knock detection. The only differ-

ence is that signal processing is performed on the signals generated from block accelerometers rather than piezoelectric pressure transducers. Joint time-frequency knock detection methods help to improve knock detection accuracy using vibration sensors [39, 50]. This measurement method has also been extended to the use of acoustic microphones for knock analysis [33].

Model-based knock detection methods are gaining attention with the possibility of integrating Field Programmable Gate Array (FPGA) for engine control [51, 52]. In this method, the end-gas auto-ignition is modeled with the solution of a detailed chemical kinetic mechanism [53, 54]. The drawback of this approach are: 1. it is computationally expensive, 2. accurate reaction mechanisms are not available for all fuels in the market, and 3. the development of reaction mechanisms for commercial fuels is not easy [55, 56]. This method becomes more computationally extensive when it is integrated with 3D computational fluid dynamics models [57], where solving thousands of reactions and transporting the hundreds of related species between zones becomes impractical for realtime implementation. Data driven machine learning methods have also been explored for knock detection and emissions prediction, however, these methods require extensive engine testing and data collection for accurate predictions [58, 59].

Another simplified approach is to implement an empirical Arrhenius model coupled with Livengood-Wu integral for knock detection [60, 61]. For this purpose, Arrhenius model coefficients need to be tuned based on experimental measurements from rapid compression machines or shock tubes. Another technique is to tune the Arrhenius coefficients with the help of detailed chemical kinetics for different pressures, temperatures, and equivalence ratios if the reaction mechanism is known. The significant drawbacks of this method are 1. it is not able to well predict the Negative Tem-

perature Coefficient (NTC) regime, and 2. the model accuracy reduces with the presence of Exhaust Gas Recirculation (EGR) and water injection used for advanced engine knock control [62, 63]. This technique has been used in literature for knock detection and control [64]. An alternative procedure is to use look-up tables [65, 66] instead of using the Livengood-Wu integral. The look-up tables are usually created based on the off-line solution of chemical reactions in a Constant-Pressure (CP) and Constant Volume (CV) reactors for a range of temperature, pressure, and fuel equivalence ratios. The model accuracy can be increased with adaptive parameter estimation schemes [65]. The model accuracy depends on the operating range that the model parameters are tuned. If the model parameters are correctly tuned, then the technique can be used for cycle-by-cycle knock detection and control.

The methods developed in the literature for knock detection have many similarities in the prediction of knock onset and intensity [2]. The goal of this work is not to develop a new knock detection method, but to focus on ASTM D6424 knock detection method used in general aviation, and compare it to the other practical methods developed in the literature: third derivative of pressure trace [35, 36, 67], and DWT [43, 48]. This analysis is performed based on Continental TSIO-520 six-cylinder engine measurements in an altitude chamber at the NRC. In-cylinder pressures and cylinder head temperatures were recorded for all cylinders and are used to calculate Knock indexes. The knock analysis was conducted with a dynamic mixture lean-out where the air/fuel ratio was increased. During each mixture sweep, in-cylinder pressure and the altitude chamber data were collected. The engine is tested at high load operating points which are subject to detonation behavior. These operating points involve high intake manifold pressures. Engine operating temperatures and oil temperatures are kept at maximum allowable limits, while in-

duction and cooling air temperatures are maintained at extreme hot day conditions for severe case testing. This work highlights the effects of pressure signal processing on the ASTM D6424 knock detection method and its robustness.

2. Experimental Setup

The experiments were performed on the Continental TSIO-520 six-cylinder, air cooled, horizontally opposed aircraft engine manufactured by Teledyne Continental Motors [68]. This engine is representative of engines used in many general aviation aircraft. The experiments were performed in the NRC altitude chamber and the chamber conditions were set for 12,000 ft. The altitude chamber provides conditioned air (pressure, temperature, and humidity) to simulate altitudes of up to 52,000 ft. A schematic of the NRC altitude chamber is shown in Fig. 1. The engine specifications are listed in Table 1. AVL GH14D recessed mounted piezoelectric pressure transducers were installed in all six cylinders to acquire in-cylinder pressure. In-cylinder pressure, cylinder head temperatures, and exhaust gas temperatures were recorded and the resolution for in-cylinder pressure measurement was 0.1 crank angle degree (CAD). For knock analysis in this work, 700 cycles were collected for each steady-state operating point.

The test procedure is the modified version of the PAFI test procedure detailed in [69]. The PAFI test procedure has evolved from ASTM D6424 [32]. The data collection was performed on the test stand to simulate take-off/maximum power and cruise conditions at 12,000 ft for two different engine speeds of 2450 and 2700 RPM as listed in Table 2. The extended version of this table is in the appendix, including the transient number (TR) which defines the specific measurement and detailed experimental conditions for take-off and cruise conditions. The engine was set at full rich ($\lambda \approx 0.7$) for each operating condition first, and the fueling rate was reduced by 5% at each

interval until knock intensity exceeds the specified limit defined in ASTM D6424 [32], and well established in PAFI [69]. The air-to-fuel equivalence ratio, λ , is the fuel ratio normalized to one at the stoichiometric mixture. During the mixture sweep, engine and altitude chamber data is collected along with the in-cylinder pressures. Each mixture lean out test has been defined as a measurement set in the appendix. The measured in-cylinder pressure is used for knock analysis.

Table 1: Continental TSIO-520 Engine Specifications

Parameter	Values
Bore \times Stroke [mm]	133 \times 101
Compression Ratio [-]	7.5
Connecting Rod Length [mm]	168
Maximum Rated Power [HP]	325
Maximum Rated Speed [RPM]	2700
Intake Valve Closing [CAD aTDC]	-140
Exhaust Valve Opening [CAD aTDC]	140
Spark Advance [CAD bTDC]	20

Exhaust gas temperature was measured using a K type thermocouple installed with manufacturer’s recommended location within 5 cm of the exhaust stack flange. Cylinder head temperatures were measured using J type thermocouples. The maximum cylinder head temperature was kept within 6° C of the manufacturer’s recommended maximum temperature limit (238° C). All cylinder head temperatures were maintained within 28° C of the specified maximum. These settings were maintained throughout the engine knock testing. The operating point is considered as a knocking operating point when 2% of the measured cycles have knock numbers of more than 10 bar

[69]. The cylinder head and exhaust gas temperatures were monitored during the tests to avoid overheating. The locations of each sensor used in this work is shown in Figure 2. For all experiments in this work, the engine spark timing was constant at 20 CAD bTDC [71]. The tests were performed with 100LL gas first and then repeated with unleaded fuel candidates A & B (see Table 3). Fuels A & B are the fuels selected amongst other fuel candidates to move on to the PAFI phase II program, which involved extensive full-scale engine and aircraft testing. These fuel candidates are being tested extensively for their high-octane, and high-heat-content to generate a comprehensive database to support the conversion of their ASTM test specification into production specifications. Both unleaded fuel candidates are oxygenated high octane number fuels and with fuel properties close to the 100LL fuel. As fuel candidate B has the lowest octane number it is used for the filter design. The experiment parity was maintained over the examined operating conditions for each tested fuel by controlling the induction air properties, effective altitude and engine cooling to the same level throughout. It was determined that the sixth cylinder experienced the most significant knock of all the six cylinders. Therefore, the knock investigations presented are for this cylinder.

3. Filtering effects

The signal processing of the measured in-cylinder pressure has a significant effect on the knock detection methods presented in this work. Not only are there various suggestions of which filter to use but also the suggestion not to use any filter but rather use the raw measured pressure signal for knock index calculations. The ASTM D6424 [32] standard does not contain any recommendation regarding the post-processing of the measured pressure signal before calculating the knock index. In the PAFI test[69], which has been developed from the ASTM D6424 standard, it is suggested that

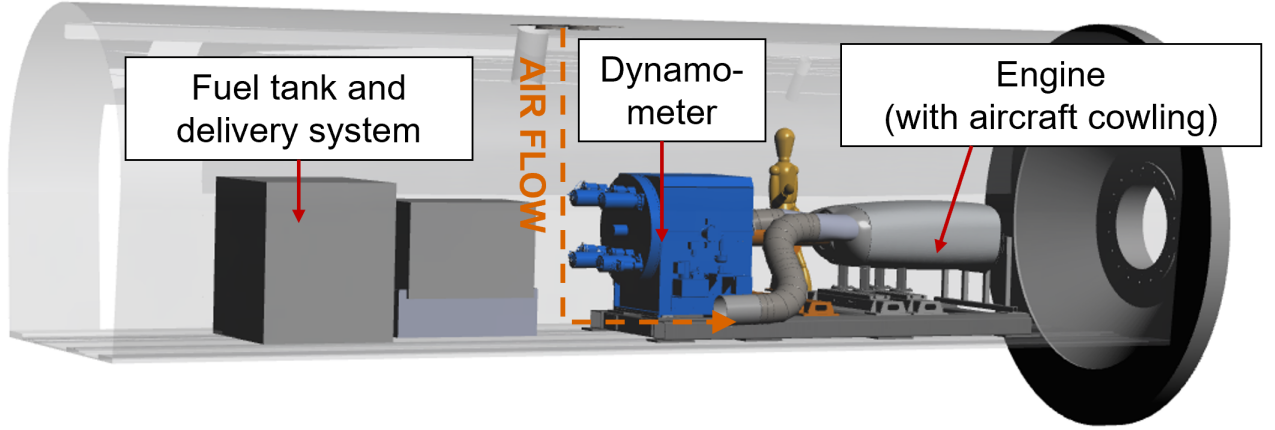


Figure 1: NRC altitude chamber layout [70]

Table 2: Engine Operating Conditions for Knock Tests

Test Cond.	Altitude [ft]	Intake Air Temperature [C]	Engine Speed [RPM]	MAP [in HG]	Cyl. Head Max. Temp. [C]
Take-Off	12,000	13.4	2700	39	237.8
Cruise	12,000	13.4	2450	29.5	237.8

Table 3: Fuel Properties

Property	Test Method	100LL	Test Fuel A	Test Fuel B
Density @ 15 C [$\frac{\text{kg}}{\text{m}^3}$]	ASTM D4052	714.5	765.3	708.2
Net Heat of Combustion [$\frac{\text{MJ}}{\text{kg}}$]	ASTM D3338	43.9	42.5	42.7
Motor Octane Number	ASTM D2700	101.9	100.5	98.8
Chemical Composition				
H (mass %)	-	15.04	12.86	15.31
C (mass %)	-	83.94	82.44	80.77
O (mass %)	-	0	2.96	3.92
N (mass %)	-	0	1.02	0
Molecular Weight	ASTM D6730	99.6	97.17	109.6

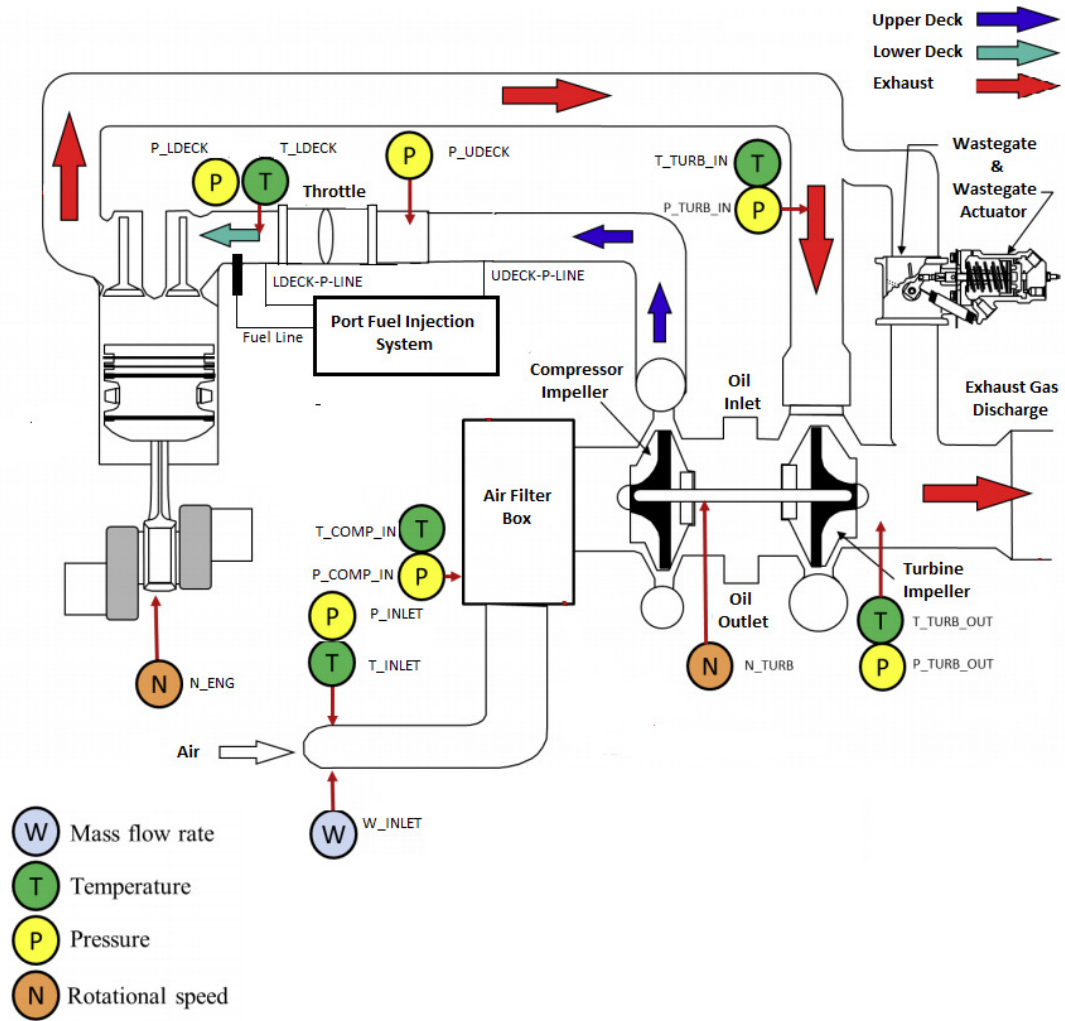


Figure 2: Engine measurement instrumentation [71]

the raw pressure data is first conditioned using a digital Finite Impulse Response (FIR) low-pass filter with cutoff frequency of 15.1 kHz. The details of the filter design were not reported in [69], which makes it difficult to compare the filter used in [69] to the one designed and implemented in this work. The designed filter will then be referenced to the unfiltered data.

3.1. Filter design

The measured in-cylinder pressure versus crank angle for low, moderate, and high knock operating cycles are shown in Figure 3. The measured moderate and high knock pressure signals show high-frequency pressure oscillations near maximum in-cylinder pressure. The location of the pressure transducer has a significant effect on the frequencies of oscillations, and the actual in-cylinder pressure oscillation intensity could be different from the measurements [43]. In this work, the in-cylinder pressure transducers were mounted vertically in the cylinder head between the intake and exhaust valves according to Teledyne Continental recommendations.

The high-frequency oscillations are analyzed from 20 CAD bTDC (spark timing) to 50 CAD aTDC. Acoustic theory [72] is used to determine the frequency of the pressure oscillations induced by engine knocking. The modes of oscillations are calculated using Draper's Equation [72, 43, 49] as

$$f_{m,n} = \frac{c\rho_{m,n}}{\pi b} \quad (1)$$

where $f_{m,n}$ is the pressure oscillation frequency in Hz, m is the order of the circumferential mode, n is the order of the radial mode, c is the speed of sound in $\frac{m}{s}$, $\rho_{m,n}$ is the factor describing the mode, and b is the cylinder bore diameter in meters. The speed of sound strongly depends on the in-cylinder charge conditions. Through proper measurement, instantaneous values can be calculated, but this is beyond the scope of this work; therefore, the speed of

sound is estimated from the calculated burned gas [72, 41]. This in-cylinder temperature was calculated using a zero-dimensional model developed in [73]. The estimated speed of sound values are being used to calculate the vibration modes using eqn. 1 to justify the Power Spectral Density (PSD) observations. For the TSIO-520 engine with the configurations listed in Table 1, the oscillation frequencies in kHz for various modes are listed in Table 4. The first circumferential mode is $\rho_{1,0}$ with $f_{1,0}=4.1$ kHz.

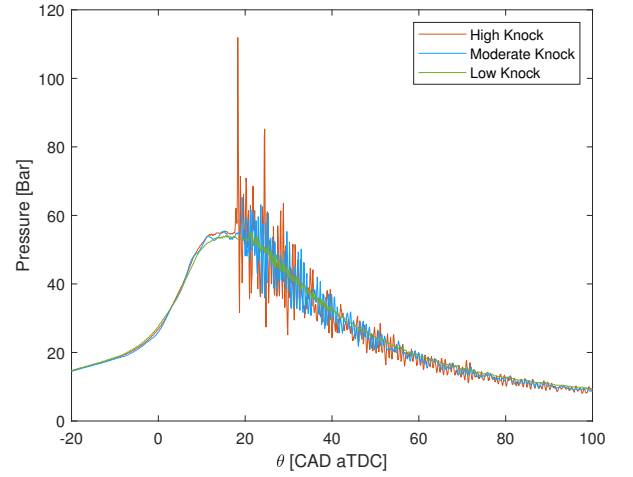
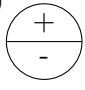
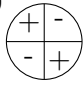
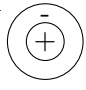




Figure 3: 0.1 CAD resolution cylinder pressure signal for Low knock, moderate knock and high knock operating condition (Fuel Type B, see take-off Tables 2 & A.5, TR700)

The PSD of the pressure signal for low, moderate, and high knock operating conditions is shown in Figure 4. Comparing the peak of the knock and high-knock PSDs to the circumferential frequencies predicted by the acoustic analysis in Table 4 indicates that the peaks at 4.2-4.6 kHz coincide with the first circumferential mode ($f_{1,0}=4.3$ kHz). Another peak is observed in the PSDs at 7.3-7.9 kHz, which corresponds to $f_{2,0}=6.9$ kHz. The difference between the observed and calculated circumferential frequency modes are mainly attributed to the assumptions made to calculate the values listed in Table 4.

In order to define low and high cut-off fre-

Table 4: Frequency modes in TSIO-520VB engine cylinder

m,n	1,0 	2,0 	0,1 	3,0 	1,1 
$\rho_{m,n}$	1.84	3.05	3.83	4.20	5.33
$f_{m,n}$ [kHz]	4.3	7.2	9.1	10.1	12.7

quencies of the band-pass filter, PSD of the high knock pressure signal is calculated using the raw measured in-cylinder pressure signal. The filter is a fifth-order Butterworth high-pass filter with a cut-off frequency of 3.8 kHz. The PSDs of the pressure signals are shown in Figure 4 for the take-off conditions listed in Table 2. A fifth-order Butterworth band-pass filter is then designed with the pass-band frequencies of 3.8-40 kHz to include those high frequencies for knock calculations. This filter is different from the FIR filter designed in [69]. The filter performance is shown in Figure 5. The filter performance is acceptable, and the filtered pressure traces are smooth, specifically in the early stages of the knock event (15-25°aTDC).

The ASTM standard requires that in addition to the high load take-off operating condition the cruise operation must also be checked for knock intensity. The PSD values of the high, moderate, and low knock pressure signals for cruise conditions is shown in Figure 6. The cruise condition operating point used to calculate the PSD values are listed in Table 2. Compared to the PSDs of the take-off high-knock pressure signals shown in Figure 4, the first circumferential mode is the dominant mode for cruise condition. For this reason, the upper cut-off frequency of the band-pass filter used for knock index calculation can be reduced to 10 kHz for cruise conditions. This is expected as the cruise condition is a lower load operating condition compared to take-off.

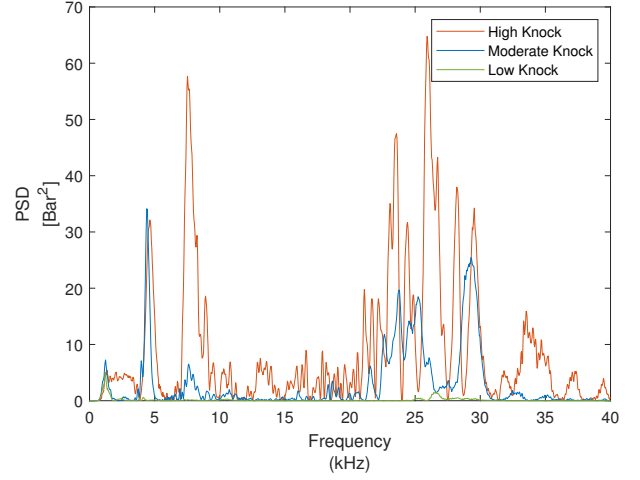


Figure 4: Power Spectral Density (PSD) of Low, moderate, and high knock operating condition for take-off conditions (Fuel Type B, see take-off Tables 2 & A.5, TR700)

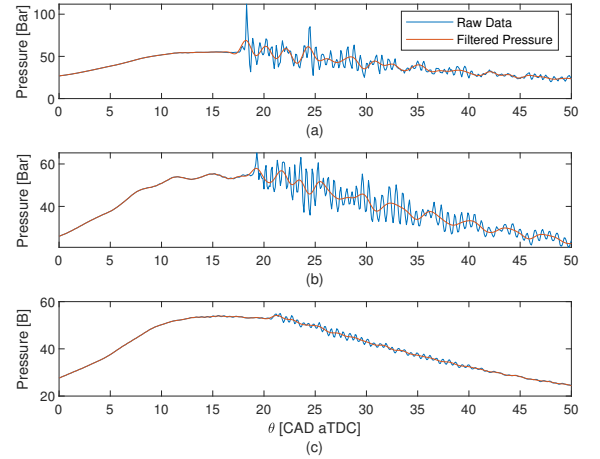


Figure 5: Comparison of the filtered pressure traces for (a) high knock, (b) moderate knock, and (c) low knock cycles (Fuel Type B, see take-off Tables 2 & A.5, TR700)

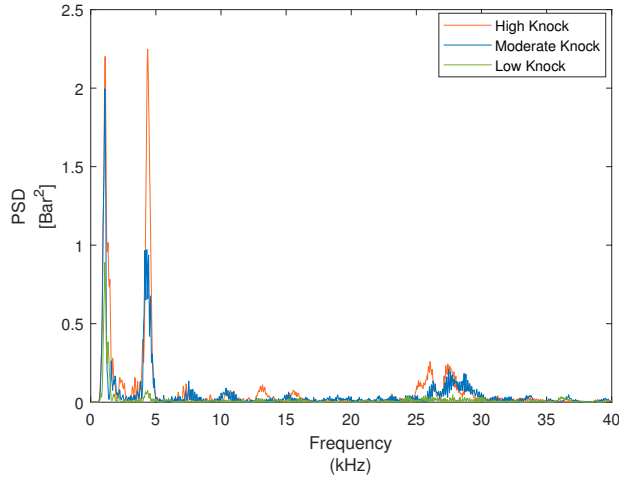


Figure 6: PSD of Low, moderate, and high knock operating cycles for cruise condition, $\lambda \approx 1$ (Fuel B, see Table 2 & A.6, TR693)

3.2. Impact of Down-Sampling

Section A1.1.3 of the ASTM D6424 [32] recommends a data sampling interval of 0.4 CAD. To reduce the computational speed requirements of the knock analysis it is valuable to see if the sample rate can be reduced. This investigation is done by down-sampling the 0.1 CAD measured data. The effects of down-sampling on the knock analysis are detailed first. Figure 7 shows the down-sampled high knock pressure single-cycle data with 0.1, 0.2, 0.4, and 0.6 CAD resolution resulting in sampling frequencies of 162, 81, 40.5, and 32.4 kHz. Figure 8 shows the corresponding down-sampled pressure traces at an engine speed of 2700 RPM. The content of the pressure signal in the 21-31 kHz range (see 0.1 CAD (162 kHz) sampled data) is aliased to the 10-20 kHz range in the 0.4 CAD (40.5 kHz) sampled data, and to the 2-10 kHz range in the 0.6 CAD (32.4 kHz) sampled data. To resolve the power spectral density of the data up to $\frac{F_s}{2}$, a sampling rate of F_s or higher is required. Therefore, a sampling rate of 80 kHz or higher is necessary to avoid aliasing because there exists high frequency content up to 40 kHz. It means that digital filtering is ineffective in removing alias-

ing if it occurs, and a sample rate of at least 0.2 CAD is needed. These results indicate that the ASTM D6424 [32] standard recommendation for sampling frequency of 0.4 CAD needs to be revised. All knock calculations performed in this work are based on the sampling rate of 0.1 CAD.

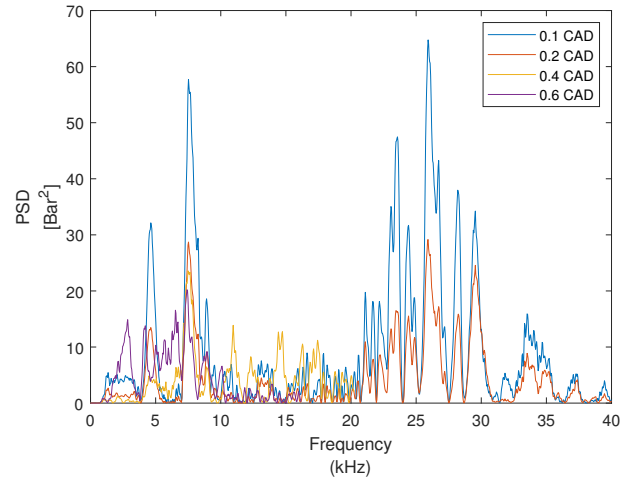


Figure 7: Effects of down sampling on Power spectral density of high knock pressure signal (Fuel Type B, see take-off Tables 2 & A.5, TR700)

4. Filtering Effects on ASTM D6424 Standard

Knock detection in aviation piston engines is typically performed based on ASTM D6424 [32]. In the ASTM D6424 standard, the knock index is determined by comparing the absolute relative pressure changes of the expansion period to the compression period. The knock index is calculated [32] as

$$KI = \sum_{i=0}^{N-1} |P_i - P_{i+1}| - \sum_{i=0}^{N-1} |P_{-i} - P_{-i-1}| (2)$$

where P_0 is the pressure value at the point that separates the expansion and compression periods, P_{-1} is the pressure value one point before P_0 , P_{+1} is the pressure value one point after P_0 , and N is the number of points either

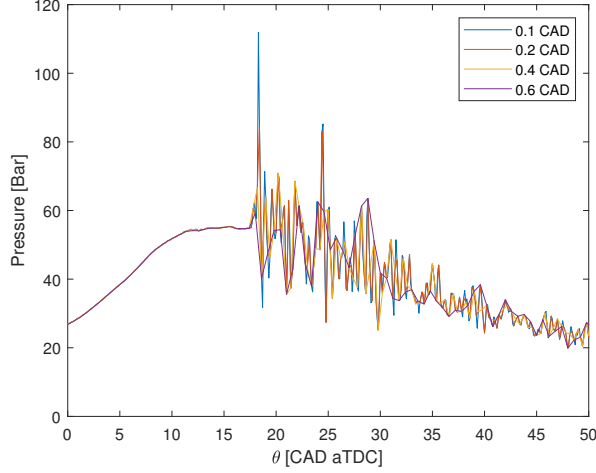


Figure 8: Effects of down sampling on high knock pressure signal (Fuel Type B, see take-off Tables 2 & A.5, TR700)

before or after P_0 . In equation 2, the sum of the absolute values of the consecutive pressure differences is summed for the compression period first. Then it is subtracted from the sum of the absolute values of the consecutive pressure differences for the expansion period. The difference in these two sums is the knock number used for knock determination. A full 70° of crankshaft rotation is recommended to determine knock number. The ASTM D6424 [32] indicates a normal cycle has a negative knock number, and knocking cycles have knock numbers of ten or higher. The visualization of P_0 and N is shown in Fig. 9.

The ASTM D6424 standard [32] does not contain any recommendation regarding the post-processing of the collected pressure for knock calculations. For at least some conditions, this leads to inaccurate knock estimation. The filtering effects on the knock magnitudes calculated based on ASTM D6424 are discussed for the unleaded fuel B first. The normalized probability density estimate of the ASTM knock numbers calculated based on the unfiltered pressure trace is compared to the ones calculated based on filtered pressure signals in Figure 10. The normalized PDE, $F_y(v)$

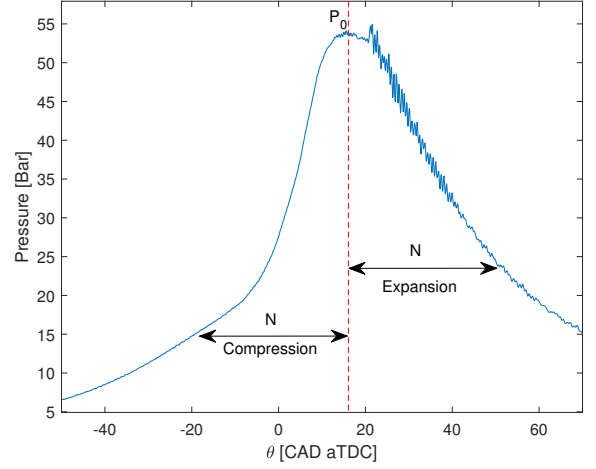


Figure 9: Pressure signal with the location of P_0 , and N

is calculated [74] as

$$F_y(v) = \frac{P(y \leq v)}{P_{max}}, -\infty < v < \infty \quad (3)$$

where $P()$ is the probability function, y is the signal under study, and P_{max} is the maximum value of the probability function.

Knock analysis based on unfiltered in-cylinder pressure concludes that 70% percent of the measured cycles experience knock (ASTM knock index greater than 10), as seen in Figure 10(b). However, examining the data closely it is known that having knock in 70% of measured cycles is not correct.

Figure 10(a) shows the normalized probability density estimate using the in-cylinder pressure trace filtered with the band pass filter with a 10 kHz upper cut-off frequency. This filter is designed based on cruise PSD analysis. The results using this filter indicate that the take-off operating point (see Table 2) is knock free, while the observations indicate this is an operating point experiences high knock cycles. Next, the in-cylinder pressure traces are filtered using the Butterworth low-pass filter with a 40 kHz cut-off frequency which indicates only 10% of the measured cycles are knocking cycles (see Figure 10). This confirms

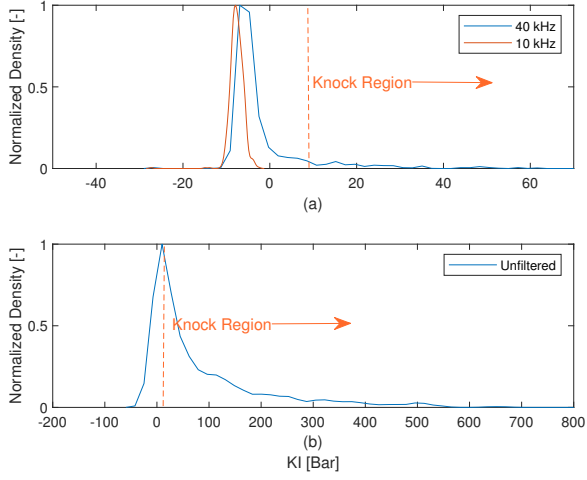


Figure 10: Probability Density Estimate of the ASTM Knock number (a) filtered pressure signal (b) unfiltered pressure signal (Fuel Type B, see take-off Tables 2 & A.5, TR700)

the results presented above for the filter design, where it is shown that frequencies up to 40 kHz are required for accurate knock detection for take-off operation. Using the cut-off frequency of 40 kHz provides a realistic percentage of knocking cycles and shows that filtering has a significant effect on the knock index when using the ASTM D6424 standard.

Figure 11 shows the combustion timing, θ_{50} , versus burn duration for an operating point with high knock measured cycles for fuel B. These combustion indexes are calculated using the measured pressure traces for 700 consecutive cycles of this operating condition. The combustion timing, θ_{50} , is defined as the crank angle of fifty percent fuel mass fraction burned [1]. Burn Duration, BD, is calculated [1] as

$$BD = \theta_{90} - \theta_{10} \quad (4)$$

where θ_{10} and θ_{90} are defined as the crank angle of 10%, and 90% fuel mass fraction burned respectively. Figure 11(a) indicates that the calculation based on unfiltered pressure signal identifies the majority of the cycles as knocking cycles. The cycles with shorter

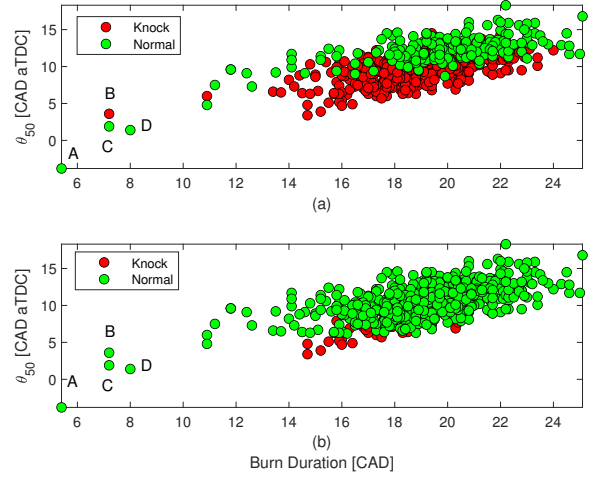


Figure 11: Combustion timing vs. Burn duration (a) unfiltered pressure signal (b) filtered pressure signal with 40 kHz cut-off frequency (Fuel Type B, see take-off Tables 2 & A.5, TR700)

burn duration and advanced combustion timing are suspect to be the knocking operating cycles. Cycles A, B, C, and D have a shorter burn duration with an advanced combustion timing compared to the other cycles shown in Figure 11. The calculated ASTM knock values for these cycles are listed in Table 5. ASTM knock values calculated based on the fifth-order Butterworth low-pass filter with a 40 kHz cut-off frequency classify cycles A, B, C, and D as knock-free cycles. While ASTM knock values calculated based on unfiltered data identify cycle B as a knocking cycle. A closer look at these cycles indicates that these cycles are suspect to auto-ignition under spark assisted compression conditions (see Figure 12), which both ASTM calculated values based on filtered and unfiltered data failed to detect. The peak heat release rate of auto-ignition cycles is higher compared to the normal cycle.

Auto-ignition under spark assisted compression ignition conditions usually leads to high in-cylinder pressure and temperatures. This combustion mode is different from a knock, or super-knock [3] and the mechanism underlying this mode of combustion without knocking is

Table 5: ASTM D6424 Knock number

Operating Cycle	A	B	C	D
ASTM Knock [Bar] (40 kHz)	-26.4	2.8	-5.68	-12.1
ASTM Knock [Bar] (Unfiltered)	-16.0	15.9	4.8	4.1

not well known [75, 76]. This mode of combustion can be distinguished from normal SI combustion using the rate of heat release, rate of pressure rise, burn duration, and maximum in-cylinder pressure as depicted in Figure 12. Figure 12 shows the pressure trace and heat release rate of the four operating cycles selected in Figure 11 and compared to a normal operating cycle. The most significant difference between these cycles and the normal cycle is the amplitude of the rate of pressure rise at combustion onset, maximum in-cylinder pressure, the maximum rate of heat release, and burn duration. The magnitude of the maximum pressure signal for cycle A is almost two times the magnitude of the maximum pressure of the normal cycle (ΔP in Figure 12). Compared to the normal cycle, the maximum heat release rate for cycles A, B, C, and D is 3.13, 2.28, 2.38, and 2.04 times higher. For cycles A, B, C, and D, the heat release rate is slow after spark ignition. This slow heat release causes an increase in pressure and temperature within the unburned gas zone, which results in the auto-ignition of the unburned mixture. However, as detailed in the literature [75], the mechanism underlying the auto-ignition under spark assisted condition without knocking yet remains unclear. The occurrence of auto-ignition under spark assisted condition can severely damage the engine due to extremely high peak pressure if not controlled by modulating spark timing or mixture strength. These results indicate that ASTM D6424 identifies these cycles as low-knock or normal cycles, which is not correct.

Next, the fuel type effects on knock distribution and intensity of a heavy knock take-

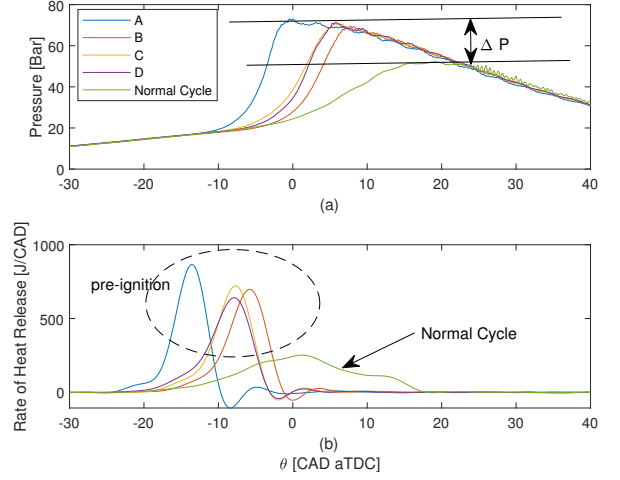


Figure 12: Combustion parameters of auto-ignition under spark assisted compression ignition conditions (Fuel Type B, see take-off Tables 2 & A.5, TR700)

Table 6: Performance Characteristics (Averaged Values)

Fuel Type	A	B	100LL
IMEP [Bar]	12.15	12.04	12.16
θ_{50} [CAD aTDC]	9.6	13.4	9.6
BD [CAD]	18.8	22	20
Cyl. Head Temp. [C]	236	236	223
Exhaust Gas Temp. [C]	876	807	862
λ	0.95	0.78	1

off operating point are investigated. Figure 13 shows the normalized probability density estimate of the ASTM knock number for the high knock operating points tested with the fuels listed in Table 3. As observed, fuel types A and B show a similar knock distribution, which is both higher than the reference 100LL knock intensity. The operating points shown in Figure 13 are collected for take-off (see Table 2) at same condition except for λ where the engine was run on a rich mixture for fuel B (see Table 6).

Figure 14 shows the combustion timing vs burn duration for the operating points investigated in Figure 13. The 95% probability of the combustion timing versus burn duration for

each operating point is calculated and shown on the same figure. The results indicate that the distribution of cycles for the 100LL fuel presents a tighter grouping, which could be indicative of the more predictable behavior of the fuel regarding combustion timing and burn duration. Fuel A presents a wider distribution, pointing towards a more correlative relationship between the two variables. The fuel B behavior seems to be in between the other two. Fuels A and B have a similar combustion timing and burn duration distributions, while the 100LL fuel distribution is less compared to fuels A and B. The Pearson Correlation Coefficient (PCC) of fuel A is relatively high, while the PCC value for the 100LL has dropped considerably. The PCC value for fuel B is also less than fuel A, but higher than 100LL. Looking now at the aspect ratio of both the combustion timing and burn duration distributions, which is a metric of how aligned the groupings are, a higher aspect ratio was observed for the fuel A. These results indicate that the level of variation of the flame propagation process varies with the fuel composition, which directly affects the knock intensity level.

The ASTM knock detection robustness is investigated next. The ASTM knock values based on unfiltered, 10 kHz and 40 kHz cut-off frequency filtered cylinder pressure are shown in Figure 15. The ASTM knock values calculated based on the unfiltered and filtered pressure signals using a fifth-order Butterworth low-pass filter with 40 kHz cut-off frequency can detect the cycles with high knock numbers; however, with different magnitudes. The 87th cycle ASTM knock value calculated based on the fifth-order Butterworth low-pass filtered pressure trace with 40 kHz cut-off frequency is 120.3 bar. In contrast, the same cycle knock value based on unfiltered pressure trace is 1615 bar, which is thirteen times higher than the values calculated based on filtered pressure trace. Ideally the large difference in knock index between knocking and regular combustion cycles

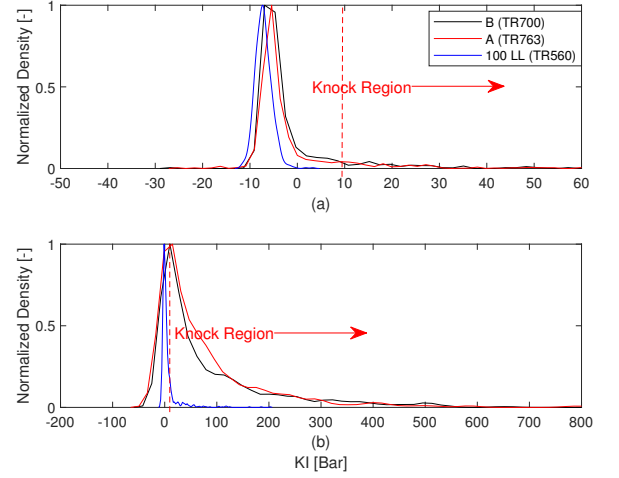


Figure 13: Experiment - Normalized Probability Density Estimate of the ASTM Knock number calculated based on (a) fifth-order Butterworth low-pass filtered pressure signal with 40 kHz cut-off frequency, and (b) unfiltered pressure signal (see take-off Table 2, Table A.1-TR560, Table A.3- TR763, Table A.5-TR700)

is desired. However, as previously described, the unfiltered data results in 70% of the cycles with a knock index greater than 10 when the unleaded fuel is used. This high percentage of false-positive knock is highly undesirable to determine if the engine is experiencing knock

The ASTM knock values calculated based on a low-pass filtered pressure signal with 10 kHz cut-off frequency detects this operating point as a normal operating point. As shown in Figure 16, cycles 87, 461, and 649 are knocking cycles while Fig. 15(a) demonstrates these cycles as knock-free cycles. Therefore, the ASTM knock numbers based on the low-pass filter with 10 kHz cut-off frequency failed to detect the known knocking cycles 87, 461, and 649 as cycles with high knock intensities.

This shows that the filtering of the pressure signal considerably changes the ASTM knock values and the knock detection results. These observations confirm that current ASTM D6424 [32] standard requires modification to allow for accurate knock index calculation when using new unleaded fuels. The

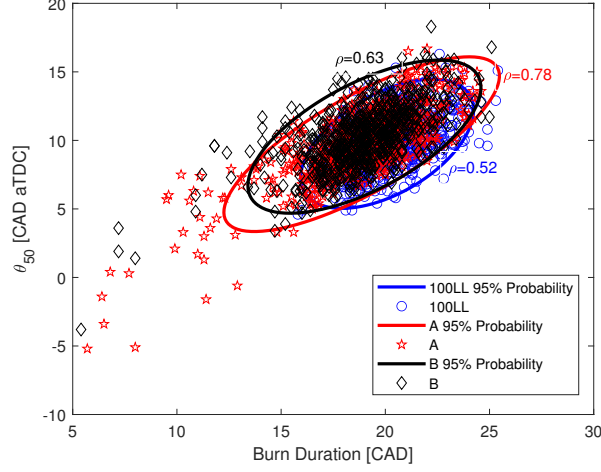


Figure 14: combustion timing vs. Burn Duration for operating points shown in Figure 13

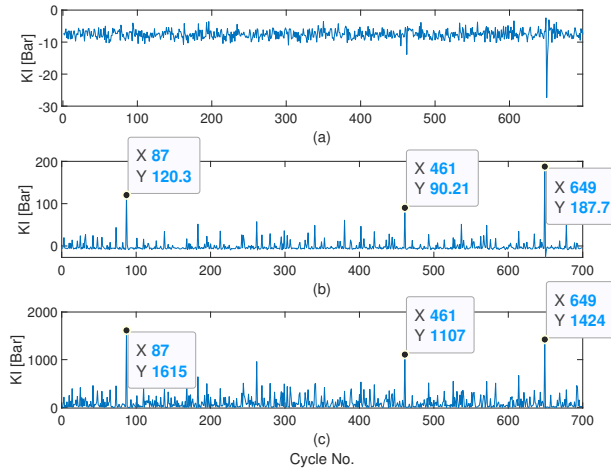


Figure 15: Cycle-by-cycle ASTM knock numbers calculated based on a fifth-order Butterworth low-pass filtered pressure signal with cut-off frequencies of (a) 10 kHz, (b) 40 kHz, and (c) ASTM knock numbers calculated based on unfiltered pressure data (Fuel Type B, see take-off Tables 2 & A.5, TR700)

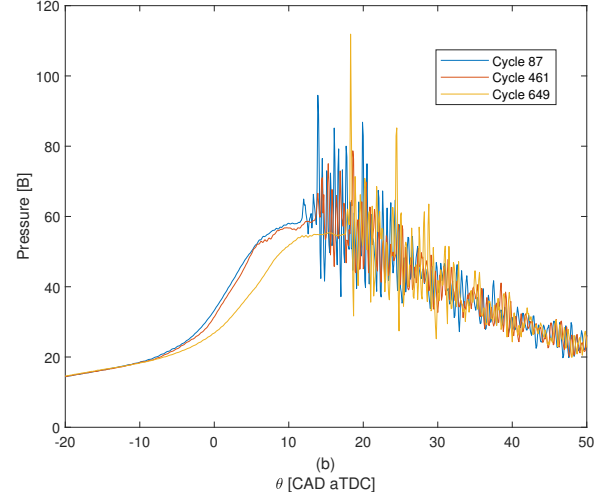


Figure 16: Pressure traces with high knock intensities (Fuel Type B, see take-off Tables 2 & A.5, TR700)

current standard of not filtering the cylinder pressure, results in over detection of knocking cycles with these two new aviation fuel candidates tested. In addition, the method is incapable of detecting cycles with auto-ignition under spark assisted compression ignition conditions experienced with unleaded fuels.

5. Mixture Sweep Knock Test Results

The calculated ASTM knock numbers based on a fifth-order Butterworth low-pass filter with a cut-off frequency of 40 kHz and the knock numbers calculated based on unfiltered pressure signals are shown in Figures 17-19 for take-off and cruise mixture lean-out experiments, respectively. The engine was set at full rich for each operating condition first, and the fueling rate was reduced gradually until knock intensity exceeds the specified limit defined in ASTM D6424 [32], and PAFI [69]. The operating points collected for these experiments are listed in Tables A.1-A.6 in the appendix.

Figure 17(a) shows that the knock values calculated based on the unfiltered pressure trace increases with mixture lean-out during take-off for all fuels tested. However, as shown in Figure 17(b), the knock intensity calculated based

on the filtered pressure trace reduces with mixture lean-out for 100LL avgas fuel. This trend opposes the outcome of the unfiltered knock analysis.

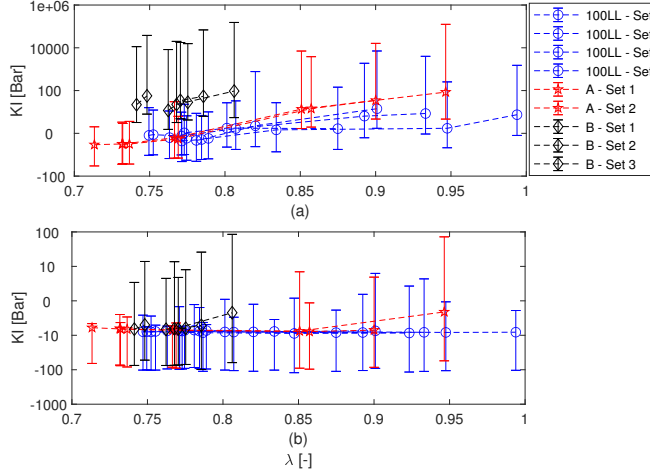


Figure 17: Averaged ASTM Knock numbers for take-off condition calculated based on (a) unfiltered pressure signal, and (b) filtered pressure data with fifth-order Butterworth low-pass filter with 40 kHz cut-off frequency (see Tables 2, A.1, A.3,& A.5)

For alternative unleaded fuel A, the measurements indicate that the average knock value reduces until λ reaches 0.83 and then the knock intensity increases with further mixture lean-out. This suggests when the filtered pressure trace is used there is an optimal fuel-air mixture to minimize the knock index. There is no expected optimal mixture and this trend is caused by the incorrect filtering cut-off frequency as shown throughout this work. This trend is not seen in the unfiltered knock index for fuel A. This shows that not only does filtering affect the magnitude of the knock index but also the trends seen during combustion variations.

The calculated knock values for fuel B indicates an increase in knock intensity during mixture lean-out when either the unfiltered or filtered data is used. However, the knock index for fuel B rises earlier in the mixture lean-out and also achieves a higher knock index when

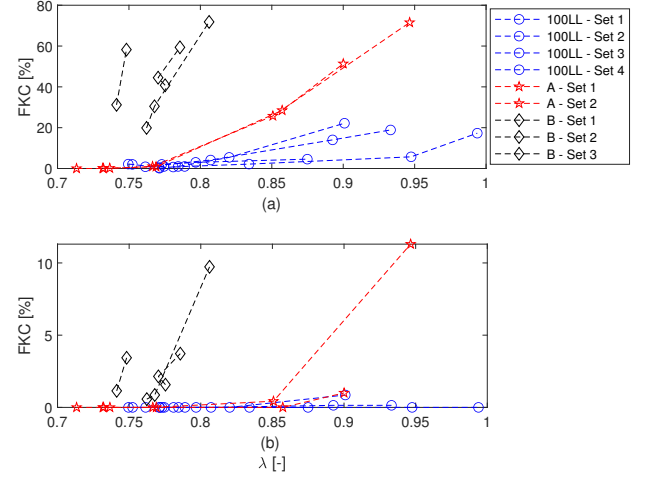


Figure 18: Fraction of knocking cycles for take-off condition calculated based on (a) unfiltered pressure signal, and (b) filtered pressure data with fifth-order Butterworth low-pass filter with 40 kHz cut-off frequency (see Tables 2, A.1, A.3,& A.5)

compared to 100LL avgas or fuel A, when either filtering option is used. In addition to the different trends seen in the mixture lean-out due to filtering, there is a significant difference in the magnitude of the ASTM knock index. For the take-off condition presented in Figure 17, the unfiltered data provides a smooth transition from negative knock index to positive values. However, both alternative unleaded fuels reach knock indexes that indicate high knock cycles ($K > 10$) even at rich operation. While the averaged knock values based on filtered data always remains at a negative knock index throughout the mixture lean-out.

The fraction of knocking cycles determined based on unfiltered and filtered pressure signal during mixture lean out is shown for take-off in Figure 18. As observed, the fraction of knocking cycles calculated based on unfiltered data is significantly higher compared to the filtered ones. The fraction of knocking cycles increases during the mixture lean out for both filtered and filtered signals. These results indicate that the pressure signal processing plays a crucial role in interpreting an operating point

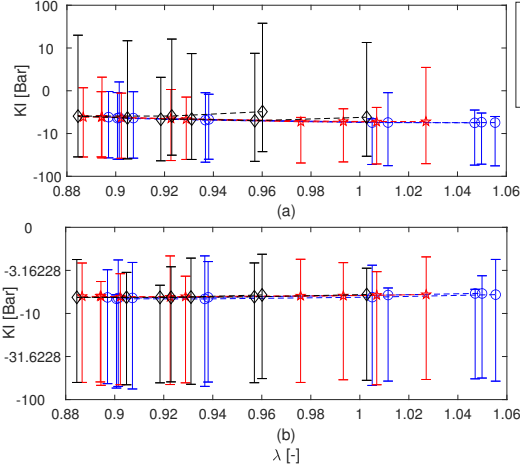


Figure 19: Averaged ASTM Knock number for cruise condition calculated based on (a) unfiltered pressure signal, and (b) filtered pressure data with fifth-order Butterworth low-pass filter with 40 kHz cut-off frequency (see Tables 2, A.2, A.4, & A.6)

as a knocking or knock-free cycle.

Next, the cruise condition mixture lean-out is investigated. The knock values calculated based on filtered pressure trace for cruise condition show the knock intensity increases for all fuels tested with mixture lean-out, as shown in Figure 19(b). This trend is opposite from knock values calculated based on unfiltered pressure signal shown in Figure 19(a) where the knock magnitudes based on unfiltered pressure trace reduces with mixture lean-out. These results indicate that all three fuels have a similar mixture lean-out trend during cruise conditions; however, the signal processing of the pressure trace significantly changes the knock values and can even reverse the trend.

The fraction of knocking cycles during mixture lean-out is investigated for cruise mixture lean-out experiments, and the results are shown in Figure 20. The knock intensity values calculated based on unfiltered pressure signal increases during mixture lean-out for fuel B (see Figure 20(a)). The fraction of knocking cycles identified based on unfiltered pressure signal for fuel A and 100LL is extremely

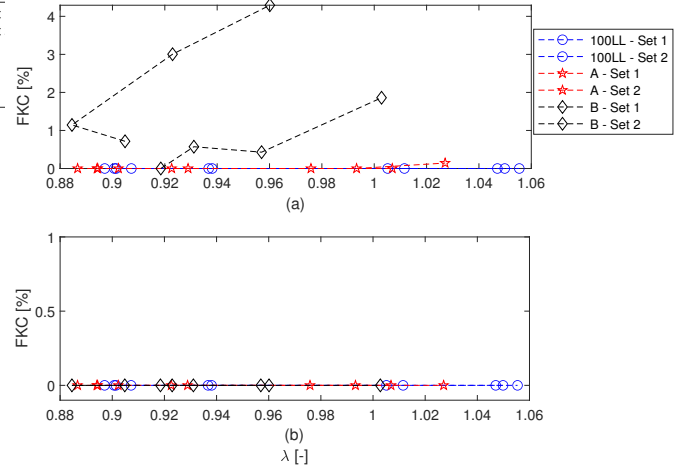


Figure 20: Fraction of knocking cycles calculated for cruise condition based on (a) unfiltered pressure signal, and (b) filtered pressure data with fifth-order Butterworth low-pass filter with 40 kHz cut-off frequency (see Tables 2, A.2, A.4, & A.6)

low. The knock values calculated based on the filtered pressure signals indicate all operating points as knock-free points.

The mixture lean-out effect on combustion parameters is discussed to understand the relationship between combustion indexes and the knock intensity. Combustion timing and burn duration values are calculated for the take-off and cruise conditions and the results are shown in Figures 21-22. The combustion timing is advanced by 3.6, 2, and 1.4 CAD for fuels A, 100 LL, and B, respectively, during the take-off mixture lean-out. The knock intensity increases with advanced combustion timing and reduced burn duration as shown in Figures 20 and 21. The knock intensity is highly sensitive to combustion timing for the unleaded fuel candidates compared to 100LL. For example, for 1.4 CAD combustion timing advance (Figure 21a) for fuel B during take-off mixture lean-out, the knock intensity (Figure 17a) increases almost nine times, considering ASTM knock numbers calculated based on unfiltered pressure trace. The combustion timing is retarded during cruise mixture lean-

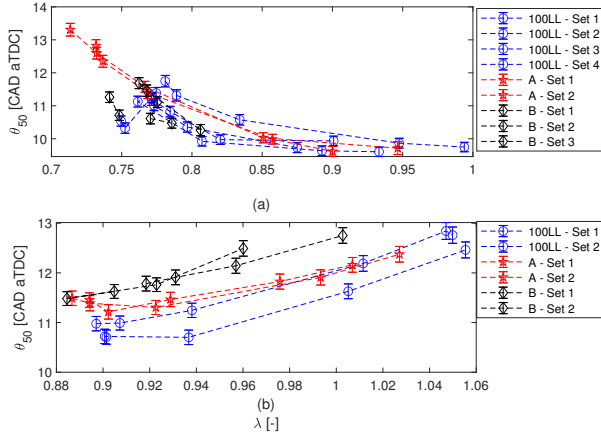


Figure 21: Averaged combustion timing (a) take-off, and (b) cruise during mixture lean-out (see Tables 2, A.1-A.6)

out with increased burn duration for all tested fuels. With retarded combustion timing and increased burn duration, the knock intensity will also be reduced. These observations are consistent with the literature [77, 78, 79]. This confirms the knock index trends seen with the ASTM knock index using the unfiltered pressure trace is capturing the correct trends during mixture lean-out.

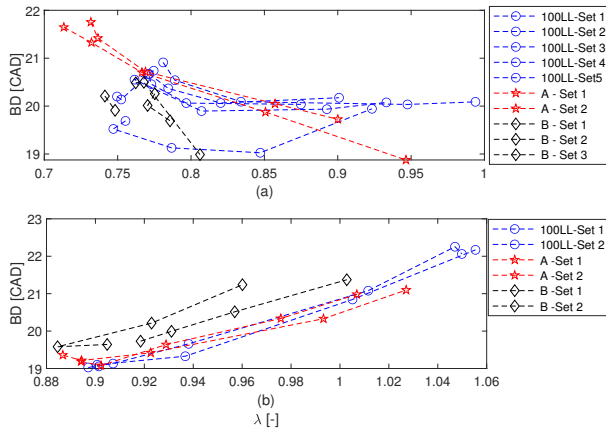


Figure 22: Averaged burn duration (a) take-off, and (b) cruise during mixture lean-out (see Tables 2, A.1-A.6)

The effects of fuel mixture lean-out on IMEP is shown in Figure 23. The engine IMEP with

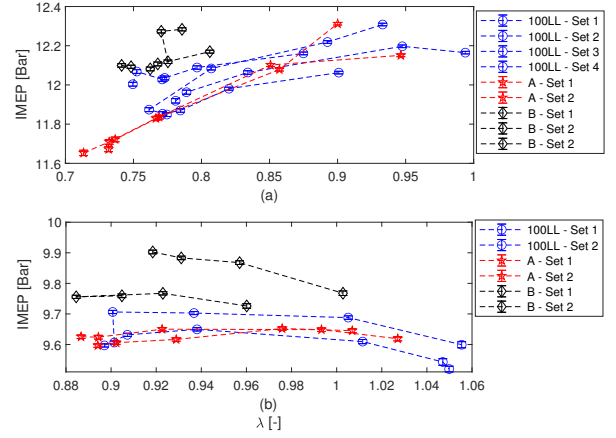


Figure 23: Averaged IMEP (a) take-off, and (b) cruise during mixture lean-out (see Tables 2, A.1-A.6)

fuels A and B are within the same range as the reference 100LL fuel. The difference between the engine IMEPs for fuel types A, B, and 100LL is mainly attributed to the fuel properties, the fuel lower heating values, and the fueling rate. IMEP slightly increases during take-off mixture lean-out; however, the IMEP values are reduced during cruise mixture lean-out. The combustion timing is advanced during take-off with mixture lean-out, as shown in Figure 21. With advanced combustion timing, expansion work increases leading to increased IMEP. For cruise conditions, the combustion timing is retarded with mixture lean-out, which reduces the expansion work. Retarding the combustion timing is an effective method for knock intensity reduction as this reduces the peak pressure and end-gas temperature; however, it could have an adverse effect on engine output power and fuel efficiency. Techniques like EGR [80] and water injection [62, 81] can be used for combustion timing and knock control in aviation SI engines. Both methods lower flame temperature and speed, so giving useful reductions in knock intensity with delayed combustion timing. These results indicate that one major challenge for aviation SI engines is to optimize combustion timing considering engine knock tendency. Therefore, to meet future

general aviation fuel economy and emission reductions, knock phenomenon in boosted low-speed general aviation piston engines need to be well understood.

5.1. Comparison with Other Knock Methods

The mixture sweep knock test results are also calculated using the third derivative of the pressure signal [35, 36, 67] and Discrete Wavelet Transform (DWT) [43, 48]. The method of third derivative of pressure signal is one effective robust pressure-based method used in commercial software [82] for knock detection and analysis. This method is based on the rate of change of pressure trace curvature over the period that auto-ignition occurs [35]. End-gas auto-ignition is associated with an abrupt increase in pressure trace following by a narrow pressure peak due to rapid heat loss. A rapid change from positive to negative curvature is associated with a large negative third derivative of pressure signal [36, 67]. However, a major problem with differentiating the pressure signal is the measurement noise. Pressure signal is filtered first as differentiation is a noise amplifying process. Fig. 24 shows the variation in third derivative of pressure signal for the pressure signals shown in Fig. 3.

The DWT method is a reliable frequency-based analysis method for knock detection as it includes the knock signal history at a discrete scale within a predefined crank-angle window. This frequency-based method is suitable for real-time knock detection and control in internal combustion engines [43]. DWT is computationally efficient as the discrete wavelet decomposition needs to be done for the knock frequency band only. In this work, DWT with a Daubechies-8 (16 coefficients) basis function, is used to analyze the knock quantity of the pressure signal [43]. The DWT is one way to represent a signal by using digital filtering techniques. Traditionally low-pass and high-pass, with the finite impulse response, are used. In this work, a three-level filter bank is created where the signal is decomposed into the

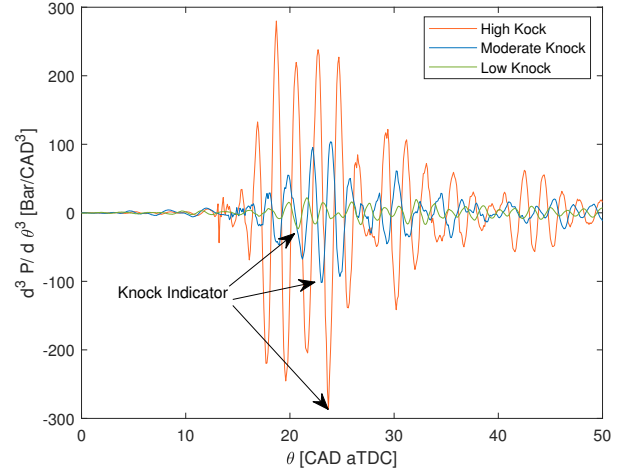


Figure 24: Comparison of the third derivative of pressure signal (Fuel Type B, see take-off Tables 2 & A.5, TR700)

high frequency and low-frequency coefficients [83, 84]. The classical DWT is computationally efficient; however, the DWT method with Daubechies is not recommended for a system with high measurement error [43].

A comparison during take-off is made between knock values calculated based on ASTM D6424 (Figure 17), the third derivative of pressure signal (Figure 25(a)) and DWT (Figure 26(a)). The ASTM knock number values calculated based on the unfiltered pressure data have the same increasing trend seen with the third derivative of the pressure signal and DWT during mixture lean-out. Additionally, when using the unfiltered data, the ASTM knock index matches the trends seen in the knock index of the third derivative of pressure and DWT for the individual fuels. A similar result can be seen for the cruise condition, where the unfiltered ASTM D6424 knock index (Figures 19), the third derivative of pressure knock index (Figure 25(b)), and the DWT knock index (Figure 26(b)) match. Again this suggests the ASTM knock values calculated based on unfiltered data are better suited to capture the correct trends during mixture lean-out.

Although the trend is more acceptable for

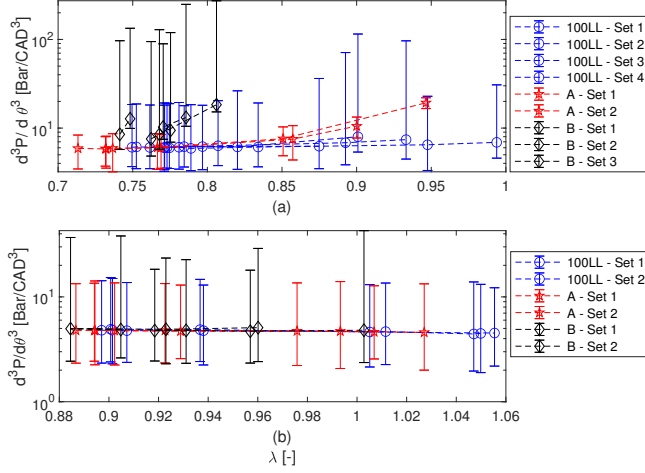


Figure 25: Averaged third derivative of pressure signal calculated based on filtered pressure data using a fifth-order Butterworth low-pass filter with 40 kHz cut-off frequency (a) take-off, (b) cruise (see Tables 2, A.1-A.6)

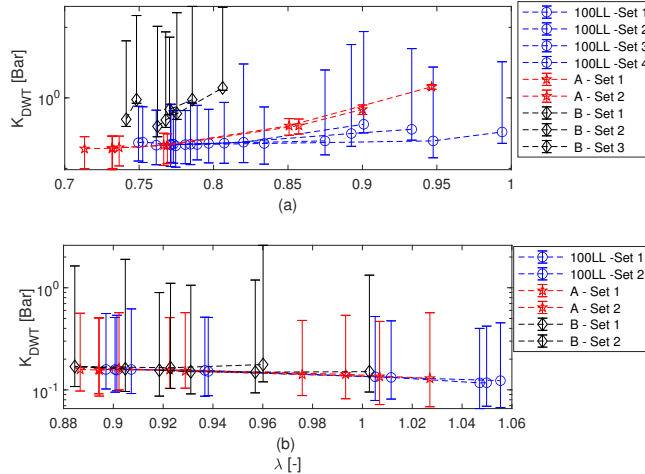


Figure 26: Averaged DWT knock index of (a) take-off, (b) cruise (see Tables 2, A.1-A.6)

ASTM knock numbers calculated based on unfiltered pressure trace, the estimated values are high. For example, ASTM knock values calculated based on unfiltered pressure trace for transient number 700 listed in Table A.5 detects cycle no. 149 and 603 as cycles with high knock numbers (ASTM Knock Number of 15 & 18 Bar, respectively). However, A closer look at these cycles (Figure 27) reveals that they are representative of normal (knock free) engine operation.

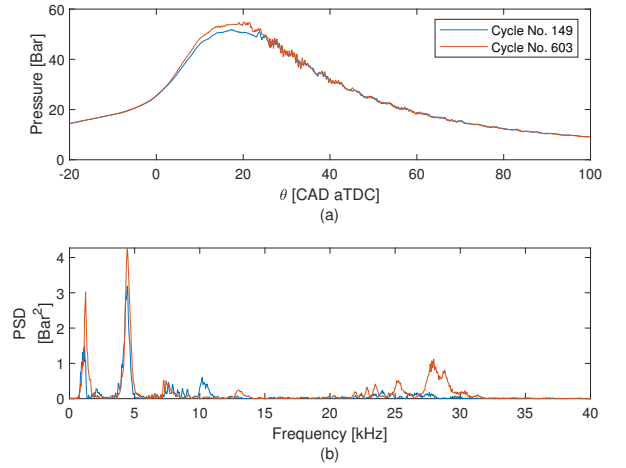


Figure 27: (a) Pressure traces (b) Power Spectral Density of corresponding pressure signals (Fuel Type B, see take-off Tables 2 & A.5, TR700)

6. Conclusions

The ASTM D6424 method is the standard used in the aviation industry for knock detection and engine certification. This work explored the impact of using unleaded aircraft fuels with this standard knock index calculation. Using measurements from the TSIO-520 engine tested at the NRC altitude chamber at a simulated altitude of 12,000 ft allowed for various knock indexes and data processing options to be explored with the standard 100LL avgas and two alternative unleaded candidates. The effects of post-processing of the pressure signal on knock detection were detailed for the

ASTM knock detection standard. It is found that the post-processing of the pressure signal significantly affects the calculated knock values, and appropriate pressure signal processing needs to be completed before the implementation of the knock detection algorithm. One improvement to the ASTM standard is the need for the minimum sampling frequency to be increased to least 0.2 CAD if aliasing is to be avoided. The results indicate that knock values calculated based on unfiltered pressure data per ASTM D6424 recommendations are not accurate and over-predict the number of knocking cycles. The use of a Butter-worth filter with a cut-off frequency of 40 kHz has enabled the accurate detection of knocking cycles when the ASTM D6424 standard is used.

During mixture lean-out tests, the proposed filter was tested against the standard unfiltered data implementation of the ASTM knock detection method. It was discovered that the application of different post-processing methods not only change the magnitude of the knock index but also change the trend seen as the mixture is changed. The results of the ASTM knock detection method were then compared to the third derivative of pressure knock and DWT knock indexes, where the ASTM knock method using the unfiltered data matched the trends seen in the other two knock detection methods. However, the magnitude of the ASTM knock index suggested that many cycles were high knock cycles as they were above the currently recommended threshold in the ASTM D6424 standard. This suggests the unfiltered pressure signal should be used to capture the correct trends in knock changes; however, the threshold that determines knocking cycles from regular cycles must be updated. The value of this threshold will require additional engine testing on various engines to determine a knock intensity threshold that works universally. Also, ASTM D6424 cannot detect cycles with auto-ignition under spark assisted conditions experiencing high maximum

in-cylinder pressure that can damage the engine instantaneously, and the ASTM standard recommendations regarding sampling frequency need to be modified. Therefore, further studies are required for pressure signal processing prior to the implementation of the ASTM D6424 knock detection method for new unleaded fuel candidates.

7. Acknowledgments

Funding by Mitacs IT08540, National Research Council (NRC) of Canada, Transport Canada, Environment and Climate Change Canada, and Canadian Owners and Pilots Association (COPA) is gratefully acknowledged.

References

- [1] John Heywood. *Internal combustion engine fundamentals*. McGraw-Hill Education, 1988.
- [2] Zhi Wang, Hui Liu, and Rolf D Reitz. Knocking combustion in spark-ignition engines. *Progress in Energy and Combustion Science*, 61:78–112, 2017.
- [3] Gautam Kalghatgi. Knock onset, knock intensity, superknock and preignition in spark ignition engines. *International Journal of Engine Research*, 19(1):7–20, 2018.
- [4] Gautam T Kalghatgi. The outlook for fuels for internal combustion engines. *International Journal of Engine Research*, 15(4):383–398, 2014.
- [5] Fabian Hoppe, Benedikt Heuser, Matthias Thewes, Florian Kremer, Stefan Pischinger, Manuel Dahmen, Manuel Hechinger, and Wolfgang Marquardt. Tailor-made fuels for future engine concepts. *International Journal of Engine Research*, 17(1):16–27, 2016.
- [6] James C Peyton Jones, Saeed Shayestehmanesh, and Jesse Frey. Parametric modelling of knock intensity data using a dual log-normal model. *International Journal of Engine Research*, 21(6):1026–1036, 2020.
- [7] http://www.hc-sc.gc.ca/ewh-semt/pubs/contaminants/prms_lead-psgr_plomb/index_longdesc2-eng.php.
- [8] Gayle Ratliff, Christopher Sequeira, Ian Waitz, Melissa Ohsfeldt, Theodore Thrasher, Michael Graham, Terence Thompson, M Graham, and T Thompson. Aircraft impacts on local and regional air quality in the united states. *PARTNER report (Report No. PARTNER-COE-2009-002)*, 2009.

- [9] Edward Carr, Mark Lee, Kristen Marin, Christopher Holder, Marion Hoyer, Meredith Pedde, Rich Cook, and Jawad Touma. Development and evaluation of an air quality modeling approach to assess near-field impacts of lead emissions from piston-engine aircraft operating on leaded aviation gasoline. *Atmospheric Environment*, 45(32):5795–5804, 2011.
- [10] R. E. Wilkinson. Research results unleaded high octane aviation gasoline. *CRC Project No. AV-7-07*, 2010.
- [11] <https://www.faa.gov/about/initiatives/av-gas/archive/2012-10-05/>.
- [12] Federal Aviation Administration. Piston aviation fuels initiative – future unleaded aviation gasoline. *power-point presentation*, page 27, 2017.
- [13] Thanikasalam Kumar, Rahmat Mohsin, Zulkipli Abd. Majid, Mohammad Fahmi Abdul Ghafir, and Ananth Manickam Wash. Experimental study of the anti-knock efficiency of high-octane fuels in spark ignited aircraft engine using response surface methodology. *Applied Energy*, 259:114150, 2020.
- [14] Nadir Yilmaz and Alpaslan Atmanli. Sustainable alternative fuels in aviation. *Energy*, 140:1378 – 1386, 2017. Advanced Energy Technologies in Aviation.
- [15] Dave Atwood. Full-scale engine detonation and power performance evaluation of swift enterprises 702 fuel. Technical report, Office of Aviation Research and Development, Federal Aviation Administration, 2009.
- [16] Thanikasalam Kumar, Rahmat Mohsin, Zulkipli Abd Majid, Mohammad Fahmi Abdul Ghafir, Nur Kamilah Yusuf, JeYoung Kim, Ananth Manickam Wash, and Dzulkarnain Mohd Sahri. Response surface methodology application in optimization of performance and exhaust emissions of ron 98, aviation gasoline 100ll and the blends in lycoming o-320 engine. *Fuel*, 256:115909, 2019.
- [17] Caio H Rufino and Janito V Ferreira. Study on the efficiency of a spark-ignition variable displacement and compression ratio engine. *International Journal of Engine Research*, page 1468087420944345, 2020.
- [18] Jiaying Pan, Lin Chen, Haiqiao Wei, Dengquan Feng, Sili Deng, and Gequn Shu. On autoignition mode under variable thermodynamic state of internal combustion engines. *International Journal of Engine Research*, 21(5):856–865, 2020.
- [19] David H Atwood and Kenneth J Knopp. Evaluation of Reciprocating Aircraft Engines with Unleaded Fuels. Technical report, SYPORT SYSTEMS INC BRIDGEWATER NJ, 1999.
- [20] US Department of Transportation. Detonation testing in reciprocating aircraft engines. *Federal Aviation Administration*, (AC 33.47-1):6, 1988.
- [21] Kimitoshi Tanoue, Yuichi Chado, Taishu Jimoto, Takashi Nomura, Fumio Shimada, and Jun Hashimoto. Effect of autoignition characteristics of fuels on knocking properties. *International Journal of Engine Research*, 17(6):666–676, 2016.
- [22] Standard Test Method for Motor Octane Number of Spark-Ignition Engine Fuel, ASTM D2699, 2013.
- [23] Standard Test Method for Research Octane Number of Spark-Ignition Engine Fuel, ASTM D2700 , 2009.
- [24] Standard Test Method for Supercharge Rating of Spark-Ignition Aviation Gasoline, ASTM D909, 2018.
- [25] I Baxter and B Yeo. An International Historic Mechanical Engineering Landmark: The Waukesha CFR Fuel Research Engine. 1980. *American Society of Mechanical Engineers: Waukesha, WI*.
- [26] Christopher Brock and David L Stanley. The cooperative fuels research engine: applications for education and research. *Journal of Aviation Technology and Engineering*, 2(1):7, 2012.
- [27] Cesar Gonzalez and Richard L Jesik. The multi-fuel general aviation piston engine. *SAE transactions*, pages 257–282, 2000.
- [28] Rik D Meininger, Chol-Bum M Kweon, Michael T Szedlmayer, Khanh Q Dang, Newman B Jackson, Christopher A Lindsey, Joseph A Gibson, and Ross H Armstrong. Knock criteria for aviation diesel engines. *International Journal of Engine Research*, 18(7):752–762, 2017.
- [29] B Lee, YG Guezennec, and G Rizzoni. Estimation of cycle-resolved in-cylinder pressure and air-fuel ratio using spark plug ionization current sensing. *International Journal of Engine Research*, 2(4):263–276, 2001.
- [30] Ming Jia, Eric Gingrich, Hu Wang, Yaopeng Li, Jaal B Ghandhi, and Rolf D Reitz. Effect of combustion regime on in-cylinder heat transfer in internal combustion engines. *International Journal of Engine Research*, 17(3):331–346, 2016.
- [31] Ying Wang and Longbau Zhou. Investigation of the detection of knock and misfire of a spark ignition engine with the ionic current method. *Proceedings of the Institution of Mechanical Engineers, Part D: Journal of Automobile Engineering*, 217(7):617–621, 2003.
- [32] Standard Practice for Octane Rating Naturally Aspirated Spark Ignition Aircraft Engines. Technical report, ASTM D 6424, 2016.
- [33] Arsham J Shahlari, Eric Kurtz, Chris Hocking, and Simon Antonov. Correlation of cylinder pressure-based engine noise metrics to measured microphone data. *International Journal of Engine Research*, 16(7):829–850, 2015.
- [34] Klaas Burgdorf and Ingemar Denbratt. Compar-

- ison of cylinder pressure based knock detection methods. *SAE transactions*, pages 1357–1374, 1997.
- [35] MD Checkel and JD Dale. Computerized knock detection from engine pressure records. *SAE transactions*, pages 221–231, 1986.
 - [36] MD Checkel and JD Dale. Testing a third derivative knock indicator on a production engine. Technical report, SAE Technical Paper, 1986.
 - [37] Hiromitsu Ando, Atsushi Nishiyama, Yoshihiro Wachi, Kazunari Kuwahara, Yasuyuki Sakai, and Takashi Ohta. Heat release rate and cylinder gas pressure oscillation in low and high speed knock. Technical report, SAE Technical Paper, 2015.
 - [38] José Carlos Zavala and Charles Folkerts. Knock detection and estimation based on heat release strategies. Technical report, SAE Technical Paper, 2011.
 - [39] Bahman Samimy and Giorgio Rizzoni. Engine knock analysis and detection using time-frequency analysis. *SAE transactions*, pages 764–775, 1996.
 - [40] Ricardo Novella, Benjamín Pla, Pau Bares, and Irina Jiménez. Acoustic characterization of combustion chambers in reciprocating engines: An application for low knocking cycles recognition. *International Journal of Engine Research*, page 1468087420980565, 2020.
 - [41] Kwang Min Chun and Kyung Woon Kim. Measurement and analysis of knock in a SI engine using the cylinder pressure and block vibration signals. *SAE transactions*, pages 56–62, 1994.
 - [42] Paulius V Puzinauskas. Examination of methods used to characterize engine knock. Technical report, SAE Technical Paper, 1992.
 - [43] Masoud Mashkournia, Adrian Audet, and Charles Robert Koch. Knock detection and control in an HCCI engine using DWT. In *ASME 2011 Internal Combustion Engine Division Fall Technical Conference*, pages 391–399. American Society of Mechanical Engineers Digital Collection, 2011.
 - [44] Hossein Ahmadian, Gholamhassan Najafi, Barat Ghobadian, Seyed Reza Hassan-Beygi, and Seyed Salar Hoseini. Evaluation of the combustion-induced noise and vibration using coherence and wavelet coherence estimates in a diesel engine. *International Journal of Engine Research*, page 1468087419878547, 2019.
 - [45] Enzo Galloni. Dynamic knock detection and quantification in a spark ignition engine by means of a pressure based method. *Energy conversion and management*, 64:256–262, 2012.
 - [46] WR Leppard. Individual-cylinder knock occurrence and intensity in multicylinder engines. Technical report, SAE Technical Paper, 1982.
 - [47] Stephane G Mallat. A theory for multiresolution signal decomposition: the wavelet representation. *IEEE transactions on pattern analysis and machine intelligence*, 11(7):674–693, 1989.
 - [48] Jonathan M Borg, George Saikalas, Shigeru Oho, and Ka C Cheok. Knock signal analysis using the discrete wavelet transform. Technical report, SAE Technical Paper, 2006.
 - [49] Jong-Hwa Lee, Sung-Hwan Hwang, Jin-Soo Lim, Dong-Chan Jeon, and Yong-Seok Cho. A new knock-detection method using cylinder pressure, block vibration and sound pressure signals from a SI engine. *SAE transactions*, pages 1808–1819, 1998.
 - [50] Stuart Trimby, Julian F Dunne, Colin Bennett, and Dave Richardson. Unified approach to engine cylinder pressure reconstruction using time-delay neural networks with crank kinematics or block vibration measurements. *International Journal of Engine Research*, 18(3):256–272, 2017.
 - [51] David Gordon, Christian Wouters, Maximilian Wick, Feihong Xia, Bastian Lehrheuer, Jakob Andert, Charles R Koch, and Stefan Pischinger. Development and experimental validation of a real-time capable field programmable gate array-based gas exchange model for negative valve overlap. *International Journal of Engine Research*, 21(3):421–436, 2018.
 - [52] David Gordon, Christian Wouters, Shota Kinoshita, Maximilian Wick, Bastian Lehrheuer, Jakob Andert, Stefan Pischinger, and Charles R Koch. Homogeneous charge compression ignition combustion stability improvement using a rapid ignition system. *International Journal of Engine Research*, 21(10):1846–1856, 2020.
 - [53] Ruixue C Li, Guoming G Zhu, and Yifan Men. A two-zone reaction-based combustion model for a spark-ignition engine. *International Journal of Engine Research*, 22(1):109–124, 2021.
 - [54] Wenrui Wang, Yu Lu, Zhiyong Li, and Hanlin Li. Simulations of engine knock flow field and wave-induced fatigue of a downsized gasoline engine. *International Journal of Engine Research*, 22(2):554–568, 2021.
 - [55] Hiroshi Kawanabe and Takuji Ishiyama. Reduced kinetic model for the combustion of n-cetane and heptamethylnonane based on a primary reference fuel reduced kinetic model. *International Journal of Engine Research*, page 1468087420931969, 2020.
 - [56] Anand Krishnasamy, Youngchul Ra, Rolf D Reitz, and Bruce Bunting. Combustion simulations of the fuels for advanced combustion engines in a homogeneous charge compression ignition engine. *International Journal of Engine Research*, 14(2):191–208, 2013.
 - [57] Anthony Robert, Karine Truffin, Nicolas Iafrate, Stephane Jay, Olivier Colin, and Christian Angel-

- berger. Large-eddy simulation analysis of knock in a direct injection spark ignition engine. *International Journal of Engine Research*, 20(7):765–776, 2019.
- [58] Azher Razzak Witwit, Azman Yasin, Mohd Azman Abas, and Horizon Gitano. Modern methods in engine knock signal detection. *Procedia Technology*, 11:40–50, 2013.
- [59] Armin Norouzi, Masoud Aliramezani, and Charles Robert Koch. A correlation-based model order reduction approach for a diesel engine nox and brake mean effective pressure dynamic model using machine learning. *International Journal of Engine Research*, 0(0):1468087420936949, 0.
- [60] Juan J Hernández, Magin Lapuerta, and Josep Sanz-Argent. Autoignition prediction capability of the livengood–wu correlation applied to fuels of commercial interest. *International Journal of Engine Research*, 15(7):817–829, 2014.
- [61] David K Marsh and Alexander K Voice. Quantification of knock benefits from reformat and cooled exhaust gas recirculation using a livengood–wu approach with detailed chemical kinetics. *International Journal of Engine Research*, 18(7):717–731, 2017.
- [62] David Gordon, Christian Wouters, Maximilian Wick, Bastian Lehrheuer, Jakob Andert, Charles Koch, and Stefan Pischinger. Development and experimental validation of a field programmable gate array–based in-cycle direct water injection control strategy for homogeneous charge compression ignition combustion stability. *International Journal of Engine Research*, 20(10):1101–1113, 2019.
- [63] Christian Wouters, Tamara Ottenwälder, Bastian Lehrheuer, Stefan Pischinger, Maximilian Wick, Jakob Andert, and David Gordon. Evaluation of the potential of direct water injection in hcci combustion. Technical report, SAE Technical Paper, 2019.
- [64] Apeng Zhou, Ting Dong, and Ben Akih-Kumgeh. Simplifying ignition delay prediction for homogeneous charge compression ignition engine design and control. *International Journal of Engine Research*, 17(9):957–968, 2016.
- [65] Zhuyin Ren, Yufeng Liu, Tianfeng Lu, Liuyan Lu, Oluwayemisi O Oluwole, and Graham M Goldin. The use of dynamic adaptive chemistry and tabulation in reactive flow simulations. *Combustion and flame*, 161(1):127–137, 2014.
- [66] Tim Franken, Fabian Mauss, Lars Seidel, Maike Sophie Gern, Malte Kauf, Andrea Matriciano, and Andre Casal Kulzer. Gasoline engine performance simulation of water injection and low-pressure exhaust gas recirculation using tabulated chemistry. *International Journal of Engine Research*, 21(10):1857–1877, 2020.
- [67] MD Checkel and JD Dale. Pressure trace knock measurement in a current SI production engine. Technical report, SAE Technical Paper, 1989.
- [68] <http://www.continentalmotors.aero/>.
- [69] Federal Aviation Administration. Detonation Test Methodology DRAFT PAFI-DTM-001. Technical report, 2016.
- [70] Pervez Canteenwalla. Test-bed for Piston Engine Research Overview. UofA Visit, 2017.
- [71] Continental Motor’s Inc. *Continental Aircraft Engine Operator’s Manual*.
- [72] Charles Stark Draper. The physical effects of detonation in a closed cylindrical chamber. 1935.
- [73] Khashayar Ebrahimi. Model based control of combustion timing and load in HCCI engines. 2016.
- [74] Jose Maria Giron-Sierra. *Digital Signal Processing with Matlab Examples, Volume 1: Signals and Data, Filtering, Non-stationary Signals, Modulation*. Springer, 2016.
- [75] Lin Chen, Ren Zhang, Jiaying Pan, and Haiqiao Wei. Effects of partitioned fuel distribution on auto-ignition and knocking under spark assisted compression ignition conditions. *Applied Energy*, 260:114269, 2020.
- [76] BT Zigler, PE Keros, KB Helleberg, M Fatouraie, Dim Assanis, and MS Wooldridge. An experimental investigation of the sensitivity of the ignition and combustion properties of a single-cylinder research engine to spark-assisted HCCI. *International Journal of Engine Research*, 12(4):353–375, 2011.
- [77] GT Kalghatgi. Fuel anti-knock quality-Part I. Engine studies. *SAE Transactions*, pages 1993–2004, 2001.
- [78] Zhen Liu and Rui Chen. A zero-dimensional combustion model with reduced kinetics for SI engine knock simulation. *Combustion science and technology*, 181(6):828–852, 2009.
- [79] Lin Chen, Ren Zhang, Haiqiao Wei, and Jiaying Pan. Effect of flame speed on knocking characteristics for SI engine under critical knocking conditions. *Fuel*, 282:118846, 2020.
- [80] Dominic Parsons, Simon Orchard, Nick Evans, Umud Ozturk, Richard Burke, and Chris Brace. A comparative study into the effects of pre and post catalyst exhaust gas re-circulation on the onset of knock. *International Journal of Engine Research*, page 1468087420962294, 2020.
- [81] Fabian Hoppe, Matthias Thewes, Henning Baumgarten, and Jürgen Dohmen. Water injection for gasoline engines: Potentials, challenges, and solutions. *International Journal of Engine Research*, 17(1):86–96, 2016.
- [82] <https://www.avl.com/-/indicom-indicating-software>.
- [83] Laurent Duval, Gilles Corde, and Pierre Leduc Van

- Bui Tran. Noise robust spark ignition engine knock detection with re-dundant wavelet transform. In *Proc.: International Conference on Noise and Vibration*, 2002.
- [84] Daniela Siano, Maria Antonietta Panza, and Danilo D'Agostino. Knock detection based on MAPO analysis, AR model and discrete wavelet transform applied to the in-cylinder pressure data: results and comparison. *SAE International Journal of Engines*, 8(1):1–13, 2015.

Appendix A. Appendix - Mixture lean-out experiment condition

Table A.1: 100 LL AVGAS take-off experiment condition

	TR	Fueling Rate [PPH]	λ [-]	MAP [inch Hg]	Cyl. Head Temp. [C]	Speed [RPM]
Set-1	536	188.6	0.74	38.7	224	2700
Set-1	537	188.5	0.75	38.8	224	2700
Set-1	545	188.6	0.77	38.7	222	2700
Set-1	546	185.8	0.77	38.7	223	2700
Set-1	547	179.2	0.79	38.7	226	2700
Set-1	548	160.5	0.87	38.6	233	2700
Set-2	555	192.1	0.78	39.1	220	2700
Set-2	556	190.3	0.78	39.1	221	2700
Set-2	557	179.8	0.83	38.9	225	2700
Set-2	559	160.2	0.94	38.9	230	2700
Set-2	561	111.5	0.99	39.2	223	2700
Set-3	580	189.8	0.77	38.9	226	2700
Set-3	582	186.4	0.78	38.8	229	2700
Set-3	586	177.6	0.82	38.7	234	2700
Set-3	588	162.7	0.9	38.8	235	2700
Set-4	595	184.8	0.77	38.3	224	2700
Set-4	597	188.1	0.76	38.8	229	2700
Set-4	599	177.5	0.81	38.8	229	2700
Set-4	601	160.3	0.89	38.9	235	2700
Set-4	603	157.2	0.93	39.1	232	2700

Table A.2: 100 LL AVGAS cruise experiments

	TR	Fueling Rate [PPH]	λ [-]	MAP [inch Hg]	Cyl. Head Temp. [C]	Speed [RPM]
Set-1	567	114.2	0.89	29.4	220	2450
Set-1	569	113.1	0.9	29.4	222	2450
Set-1	571	109.3	0.93	29.5	224	2450
Set-1	573	101.1	1.01	29.5	225	2450
Set-1	575	97.3	1.04	29.5	222	2450
Set-1	577	97.1	1.04	29.5	225	2450
Set-2	606	113.5	0.9	29.2	225	2450
Set-2	608	113.3	0.9	29.4	223	2450
Set-2	610	109.3	0.9	29.4	226	2450
Set-2	612	101.7	1.0	29.5	226	2450
Set-2	614	97.1	1.0	29.5	226	2450

Table A.3: Fuel A take-off experiments

	TR	Fueling Rate [PPH]	λ [-]	MAP [inch Hg]	Cyl. Head Temp.	Speed [RPM]
Set-1	732	214.3	0.73	38.8	227	2700
Set-1	734	212.8	0.73	38.8	229	2700
Set-1	736	203.6	0.76	38.8	233	2700
Set-1	738	182.1	0.85	38.8	238	2700
Set-1	741	177.1	0.90	39.2	232	2700
Set-2	755	219.1	0.71	39.1	226	2700
Set-2	757	213.3	0.73	38.9	229	2700
Set-2	759	202.7	0.76	38.8	233	2700
Set-2	761	181.2	0.85	38.8	234	2700
Set-2	763	163.1	0.94	38.8	237	2700

Table A.4: Fuel A cruise experiments

	TR	Fueling Rate [PPH]	λ [-]	MAP [inch Hg]	Cyl. Head Temp. [C]	Speed [RPM]
Set-1	744	126.3	0.88	29.4	224	2450
Set-1	746	125.2	0.89	29.4	225	2450
Set-1	748	121.1	0.92	29.4	227	2450
Set-1	750	109.6	0.99	29.4	228	2450
Set-1	752	108.9	1.02	29.4	229	2450
Set-2	767	125.6	0.89	29.2	223	2450
Set-2	769	124.5	0.90	29.3	224	2450
Set-2	771	120.8	0.92	29.3	226	2450
Set-2	773	113.7	0.97	29.4	229	2450
Set-2	775	110.2	1.0	29.5	230	2450

Table A.5: Fuel B take-off experiments

	TR	Fueling Rate [PPH]	λ [-]	MAP [inch Hg]	Cyl. Head Temp. [C]	Speed [RPM]
Set-1	667	187.7	0.77	38.7	231	2700
Set-1	669	191.2	0.77	39.1	230	2700
Set-1	671	187.6	0.78	39.1	233	2700
Set-2	682	190.7	0.74	38.7	230	2700
Set-2	684	188.2	0.74	38.8	233	2700
Set-3	696	193.1	0.76	39.1	228	2700
Set-3	698	191.4	0.76	39.2	230	2700
Set-3	700	182.2	0.80	39.1	235	2700

Table A.6: Fuel B cruise experiments

	TR	Fueling Rate [PPH]	λ [-]	MAP [inch Hg]	Cyl.Head Temp. [C]	Speed [RPM]
Set-1	674	115.2	0.90	29.3	229	2450
Set-1	676	114.3	0.88	29.4	232	2450
Set-1	678	109.8	0.92	29.4	229	2450
Set-1	680	105.6	0.96	29.5	232	2450
Set-2	687	115.3	0.91	29.6	224	2450
Set-2	689	114.2	0.93	29.7	225	2450
Set-2	691	110.7	0.95	29.6	226	2450
Set-2	693	105.3	1.00	29.6	230	2450